Supporting Information for:

Time dependent source apportionment of submicron organic aerosol for a rural site in an alpine valley using a rolling PMF window

Gang Chen[1*], Yulia Sosedova[1*], Francesco Canonaco[1,2], Roman Fröhlich[1], Anna Tobler[1,2], Athanasia Vlachou[1], Kaspar R. Daellenbach[1], Carlo Bozzetti[2], Christoph Hueglin[3], Peter Graf[3], Urs Baltensperger[1], Jay G. Slowik[1], Imad El Haddad[1], and André S.H. Prévôt[1**]

[1]Laboratory of Atmospheric Chemistry, Paul Scherrer Institute, CH-5232 Villigen PSI, Switzerland

[2]Datalystica Ltd., Park innovAARE, CH-5234 Villigen, Switzerland

[3]Empa, Swiss Federal Laboratories for Materials Science and Technology, Laboratory for Air Pollution and Environmental Technology, CH-8600 Dübendorf, Switzerland

** G.C. and Y.S. contributed equally to this manuscript*

*** Correspondence to:* André S. H. Prévôt (andre.prevot@psi.ch)

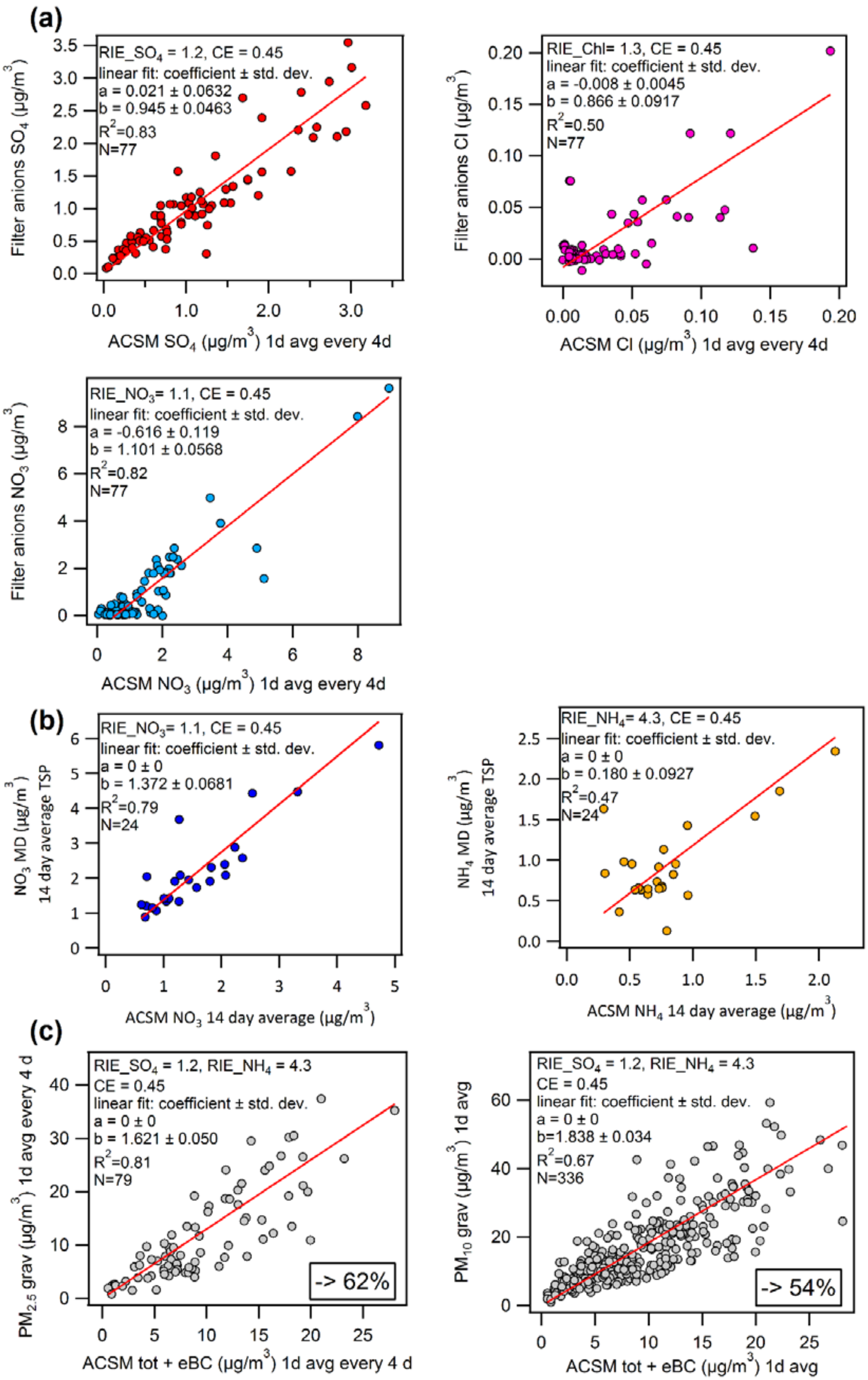
(a)
RIE_SO4 = 1.2, CE = 0.45
linear fit: coefficient ± std. dev.
a = 0.021 ± 0.0632
b = 0.945 ± 0.0463
R2=0.83
N=77
Filter anions SO4 (µg/m3)
ACSM SO4 (µg/m3) 1d avg every 4d
RIE_Chl= 1.3, CE = 0.45
linear fit: coefficient ± std. dev.
a = -0.008 ± 0.0045
b = 0.866 ± 0.0917
R2=0.50
N=77
Filter anions Cl (µg/m3)
ACSM Cl (µg/m3) 1d avg every 4d
RIE_NO3= 1.1, CE = 0.45
linear fit: coefficient ± std. dev.
a = -0.616 ± 0.119
b = 1.101 ± 0.0568
R2=0.82
N=77
Filter anions NO3 (µg/m3)
ACSM NO3 (µg/m3) 1d avg every 4d
(b)
RIE_NO3= 1.1, CE = 0.45
linear fit: coefficient ± std. dev.
a = 0 ± 0
b = 1.372 ± 0.0681
R2=0.79
N=24
NO3 MD (µg/m3)
14 day average TSP
ACSM NO3 14 day average (µg/m3)
RIE_NH4= 4.3, CE = 0.45
linear fit: coefficient ± std. dev.
a = 0 ± 0
b = 0.180 ± 0.0927
R2=0.47
N=24
NH4 MD (µg/m3)
14 day average TSP
ACSM NH4 14 day average (µg/m3)
(c)
RIE_SO4 = 1.2, RIE_NH4 = 4.3
CE = 0.45
linear fit: coefficient ± std. dev.
a = 0 ± 0
b = 1.621 ± 0.050
R2=0.81
N=79
-> 62%
PM2.5 grav (µg/m3) 1d avg every 4 d
ACSM tot + eBC (µg/m3) 1d avg every 4 d
RIE_SO4 = 1.2, RIE_NH4 = 4.3
CE = 0.45
linear fit: coefficient ± std. dev.
a = 0 ± 0
b=1.838 ± 0.034
R2=0.67
N=336
-> 54%
PM10 grav (µg/m3) 1d avg
ACSM tot + eBC (µg/m3) 1d avg

Fig. S1 Mass closure analysis of the dataset. (a) Linear correlations between the filter anions SO_4^{2-}, NO_3^- and Cl^- and the corresponding ASCM inorganic species. (b) The NO_3^- and NH_4^+ concentration measured at mini-denuders and by ACSM; (c) and between the $PM_{2.5}$ and PM_{10} fractions and NR-PM_1 defined as the sum of the total ACSM mass and the black carbon.

1 Black carbon measurement and source apportionment

The aethalometer (AE 31 model by Magee Scientific Inc.) measures eBC concentrations via the transmission of light through a sample spot at multiple wavelengths (λ = 370, 470, 520, 590, 660, 880, and 950 nm). In this study, we installed a $PM_{2.5}$ cyclone and a Nafion dryer (Perma Pure MD) in front of the sampling inlet that was shared by the AE31 and ACSM. The light absorption coefficients b_{abs} were calculated by correcting the measured attenuation coefficients for the filter loading effect (Weingartner et al., 2003). To convert optical absorption to the equivalent black carbon mass concentration eBC_{tot} in $\mu g\ m^{-3}$ (Petzold et al., 2013), the absorption coefficient at a given wavelength λ, $b_{abs}(\lambda)$ was divided by the corresponding aerosol mass absorption cross section $\sigma_{abs}(\lambda)$ in $m^2\ g^{-1}$ (Weingartner et al., 2003):

$$eBC_{tot} = b_{abs}(\lambda)/\sigma_{abs}(\lambda) \quad \textbf{\textit{(1)}}$$

with $\sigma_{abs}(470)$ = 22.9 $m^2\ g^{-1}$ and $\sigma_{abs}(950)$ = 8.8 $m^2\ g^{-1}$, as previously reported for Magadino (Herich et al., 2011).

The light absorption coefficients of eBC measured at wavelengths λ_1 = 470 nm and λ_2 = 950 nm were used to retrieve the relative contributions of traffic (eBC_{tr}) and wood burning (eBC_{wb}) to the total equivalent black carbon mass concentration eBC_{tot} (Herich et al., 2011; Sandradewi et al., 2008; Zotter et al., 2017). The two-component model implies that at a given wavelength λ the absorption coefficient b_{abs} is approximated by the sum of the absorption coefficients of eBC emitted from traffic exhaust $b_{abs,tr}$ and from wood burning $b_{abs,wb}$ (Eq. (2)), which in turn depend on λ through Eq. (3) and Eq.(4):

$$b_{abs}(\lambda) = b_{abs,tr}(\lambda) + b_{abs,tr}(\lambda) \tag{2}$$

$$\frac{b_{abs,tr}(\lambda_1)}{b_{abs,tr}(\lambda_2)} = (\frac{\lambda_1}{\lambda_2})^{-\alpha_{tr}} \tag{3}$$

$$\frac{b_{abs,wb}(\lambda_1)}{b_{abs,wb}(\lambda_2)} = (\frac{\lambda_1}{\lambda_2})^{-\alpha_{wb}} \tag{4}$$

The Ångstrom exponents for eBC from traffic $\alpha_{tr} = 0.9$ and wood burning $\alpha_{wb} = 1.68$ sources were chosen in accordance with Zotter et al. (2017) suggested for the same sampling site, Magadino.

Note that despite utilizing the aethalometer corrections proposed in (Weingartner et al., 2003), the eBC data were not fully free of filter loading artefacts, as evidenced by a discontinuity in $b_{abs}(\lambda)$ measurements on filter tape advancement. Since the filter loading effect is more pronounced at shorter wavelengths due to higher attenuation (Drinovec et al., 2015; Weingartner et al., 2003), b_{abs} measured at 470nm will have more intense signals. As a result, for winter days, when high eBC loadings triggered more frequent filter advances, artificial peaks appeared in the time series of apportioned eBC_{wb}. However, when averaging data points for the eBC diurnal cycles that we used to validate PMF solutions, transient peaks due to the filter loading artefacts had negligible effects.

2 Preparation for rolling PMF analysis

2.1 Seasonal PMF *pre-tests*

To understand the potential sources over different seasons in Magadino, PMF pre-tests were conducted based on different seasons. It provides information about the potential number of factors in different seasons, which is necessary prior to the rolling PMF analysis. In addition, the PMF solutions from rolling PMF analysis tend to be more robust if the reference profiles used to constrain are retrieved from seasonal PMF analysis. Thus, site-depended reference profiles are necessary (at least for BBOA) to get more accurate estimations of OA sources. In this study, the whole dataset was separated into five parts based on months (i.e., DJF represents winter season during December, January, and February; MAM represents spring season during March, April, and May, etc.). A preliminary "good" PMF solution (so-called base case) can be obtained for each season by following the guideline from Crippa et al. (2014) provided.

2.2 Bootstrap seasonal PMF analysis

In order to get stable reference profiles, the bootstrap re-sampling technique was applied in this study to test the stability of the base cases from seasonal PMF pre-tests. The bootstrap re-sampling randomly chooses a subset of the original matrix and replicate some of the rows/columns to create a new matrix with same-size (Efron, 1979). Given sufficient bootstrapped runs (>100) can provide the statistical uncertainty of the PMF solutions.

First, the primary factor profiles (hydrocarbon-like OA factor (HOA), BBOA) were retrieved from preliminary tests during seasonal PMF runs, while an additional local factor (LOA) was obtained in summer, then 1000 PMF runs were conducted for each season by constraining the POA factor profiles using random *a*-values with a step of 0.1 and ranging from 0-0.5. We used same criterion list as base case (as shown in Table S1) and a novel technique, t-test (Section 2.3) to define "good"

PMF runs. Then, from the averaged bootstrapped PMF solutions Fig. S6, the reference profiles can be obtained for rolling PMF analysis.

2.3 Define “good” PMF runs

The conventional PMF analysis is subjective on how to define “good” (environmentally reasonable) PMF runs. In this study, we tried to use the criteria-based approach to have a quantitative analysis on all PMF runs as suggested by (Canonaco et al., 2020). However, it is still subjective to decide the lower limit as the “good” PMF runs. Here, we used student t-test with the null hypothesis of un-correlation between the two variables (R^2 of the time series of modelled HOA vs. NO_x). For typical criteria that are based on temporal information (e.g., explained variation of m/z = 60 for BBOA), we tested for statistical significance compared to all other factors. In both cases we applied a statistical significance level of p-value ≤ 0.05. With the help of the student t-test, we retrieved comparable results with the results obtained using the approach proposed by Canonaco et al. (2020). More details of that method and comparison are in section 2.3.1. In general, this novel approach helped us to define “good” solutions with minimum subjective judgements when determining the thresholds.

2.3.1 Disadvantages of estimating season-dependent thresholds of selection criteria for rolling PMF results

Canonaco et al. (2020) proposed to define thresholds of criteria for the rolling PMF runs based on the seasonal PMF analysis. For instance, for the criterion of the R^2-Pearson between NO_x vs HOA, SoFi Pro can re-sample the time series of both BBOA factor (from averaged seasonal bootstrapped solutions) and NO_x by bootstrap. It then uses the re-sampled time series to conduct correlation analysis, which provides systematic statistic metrics, including mean, median, minimum, maximum, and $10^{th}/90^{th}$ percentile, probability distribution function, etc. Canonaco et al. (2020)

proposes to use the 10th percentile as the lower limit of the criteria in the rolling PMF analysis. This technique is useful because the re-sampled time series of the factors is relevant to the smaller time window in the rolling PMF. However, it could also cause dilemma when the thresholds are too strict to allow sufficient data coverage in the end. As shown in Fig. S2(a), the 10th percentile (R^2=0.438) caused high rejecting rate for majority of data points in fall 2013. This is potentially due to the resampling size during bootstrap of criteria is not small enough. Therefore, this technique will miss lots of data points in the model, while the t-test technique would eventually accept more data points as illustrated in Fig. S 2(b).

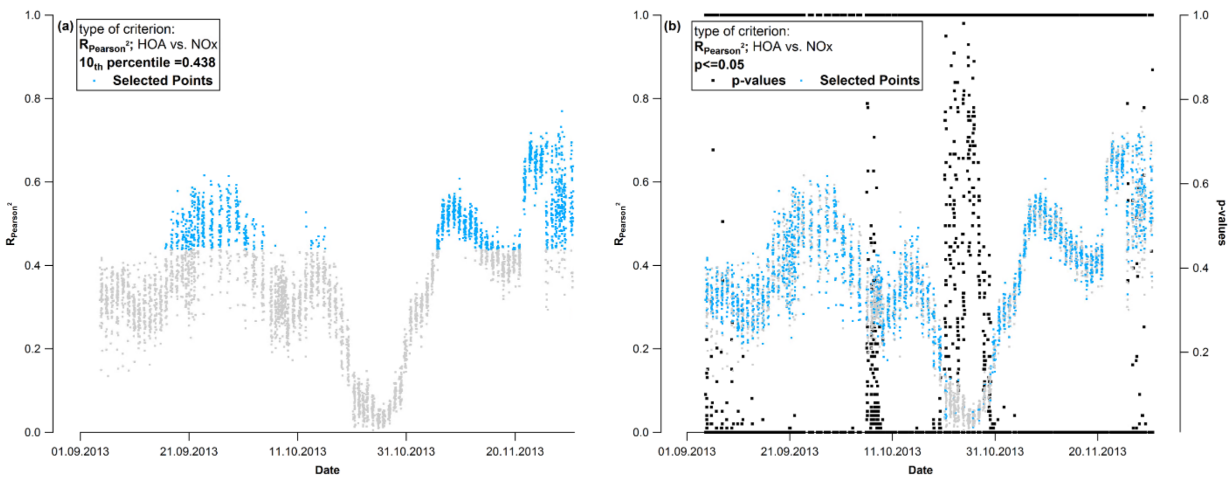

Fig. S2 Score plot the criterion for the R^2 of HOA vs NO_x in rolling PMF for fall, 2013.

2.4 Explained variation (EV) of *m/z* = 60 by BBOA

The uncertainties of aethalometer model for eBC source apportionment are very high when mass concentration of eBC_{wb} is small (Harrison et al., 2013), which was the case in summer 2014. Thus, the summer BBOA factor was poorly correlated with eBC_{wb}. In this work, we used the variation of *m/z* = 60 explained by BBOA to justify the summer solution, which is calculated using Eq. (5) (Paatero, 2010):

$$EV_{j,k} = \frac{\sum_{i=1}^{n}(|g_{ik} \cdot f_{kj}|/\sigma_{ij})}{\sum_{i=1}^{n}((\sum_{h=1}^{p}|g_{ih} \cdot f_{hj}| + e_{ij})/\sigma_{ij})} \quad \textbf{(5)}$$

Paatero (2010) suggests that if a dominant ion in a specific factor, it should explain more than 30-35% of variation of this measured variable. Canonaco et al. (2020) uses an EV of 0.25 at *m/z*=60 for BBOA as a threshold to select "good" runs for BBOA. In this study, we only selected PMF runs with EV of *m/z*=60 for BBOA that were statistic significantly larger than those of other factors by t-test with a *p*-value≤0.05. In the end, the $EV_{60,BBOA}$ values for selected PMF runs for both seasonal and rolling results are all larger than 0.4.

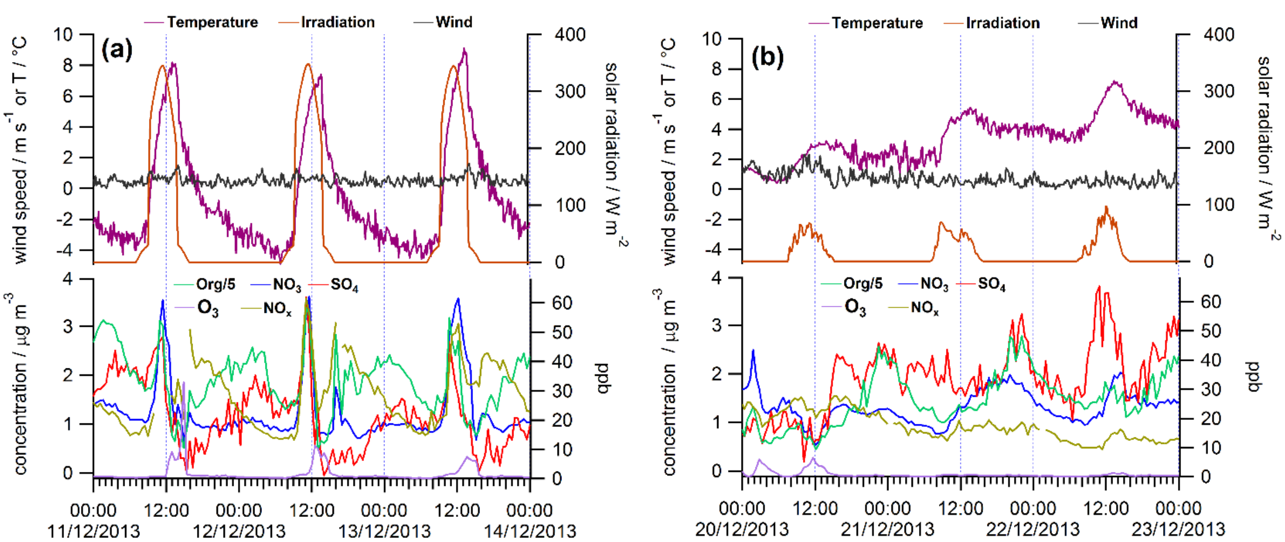

Fig. S3 Diurnal cycles of the organic, NO_3, SO_4, O_3, NO_x, and corresponding metrological data on sunny/cloudy day. (a) Transport phenomenon was observed in the noon time caused sharp enhancement of pollutants, followed by a breakthrough of a boundary layer later for dilution process. Also, the delay of the peak of the irradiation is because the fact that the monitoring station lies in the shadow of surrounding mountains. (b) No such situation was observed during cloudy days indicates that irradiation and temperature gradient might play a role in this phenomenon

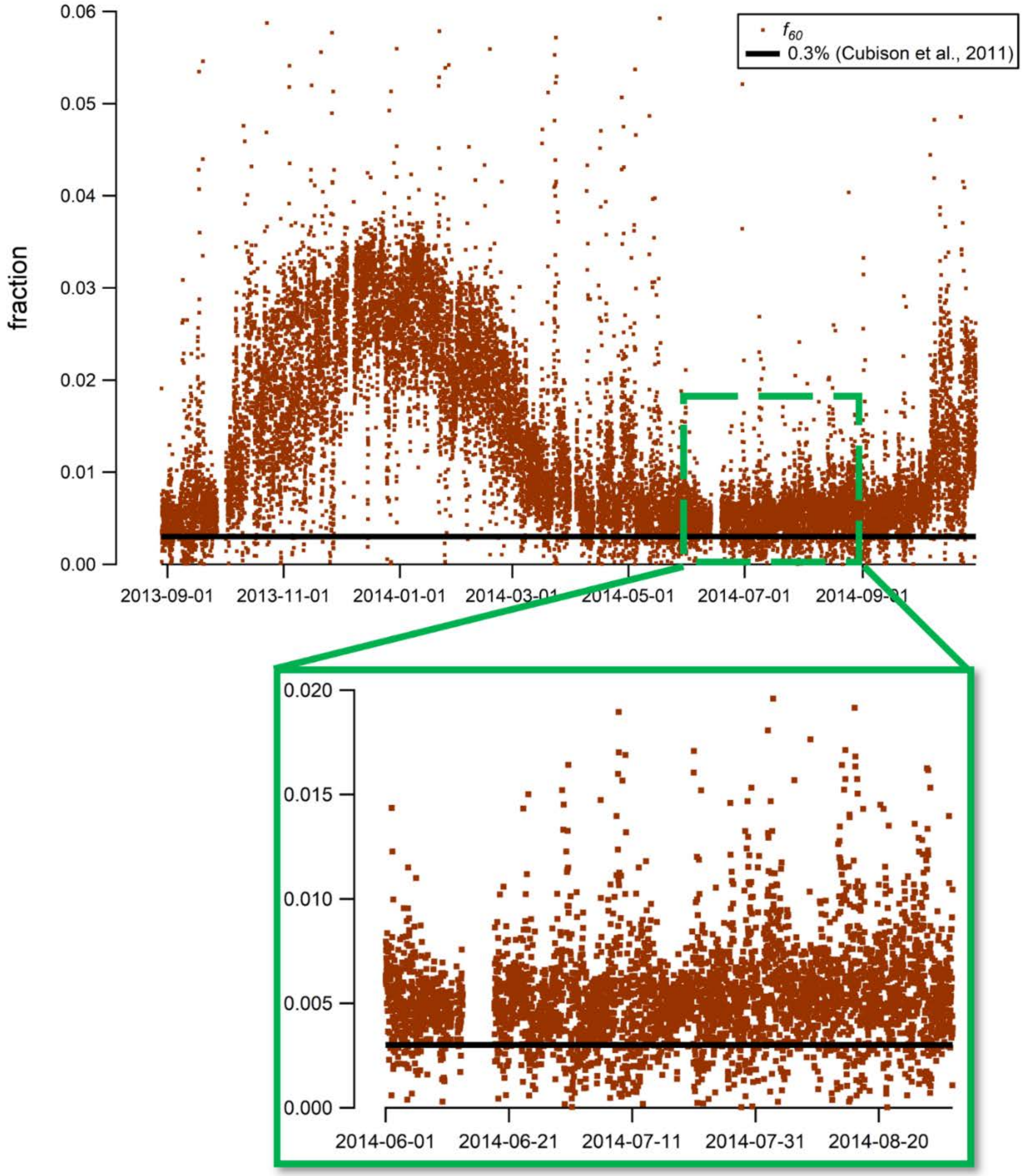

Fig. S4 Time series of the measured fraction of *m/z* = 60 (smooth the time series).

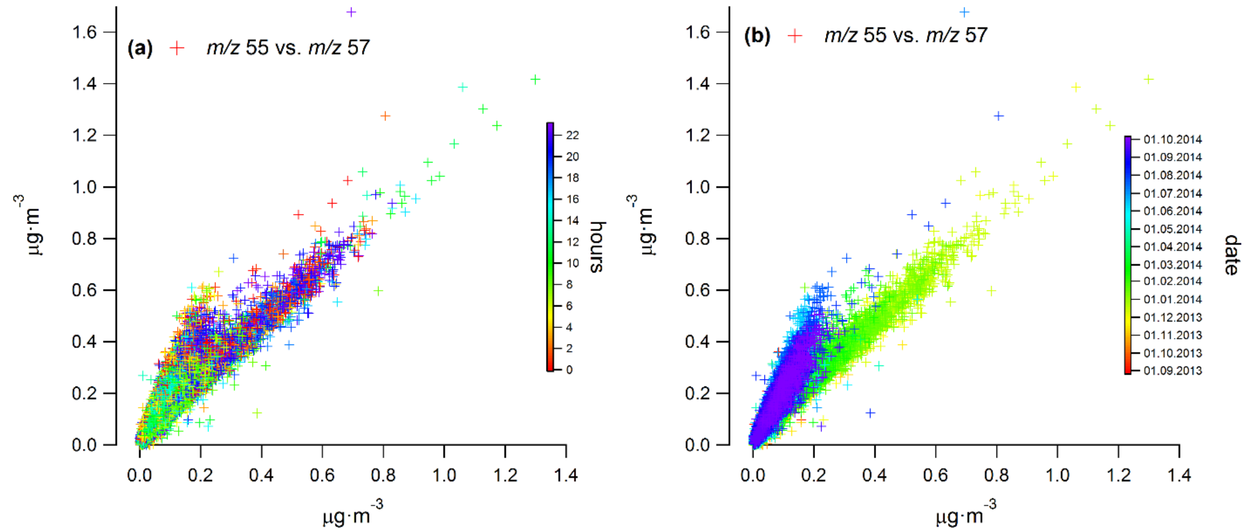

Fig. S5 Measured absolute mass concentration of *m/z*=55 vs *m/z*=57 with colour coded by hours and date/time.

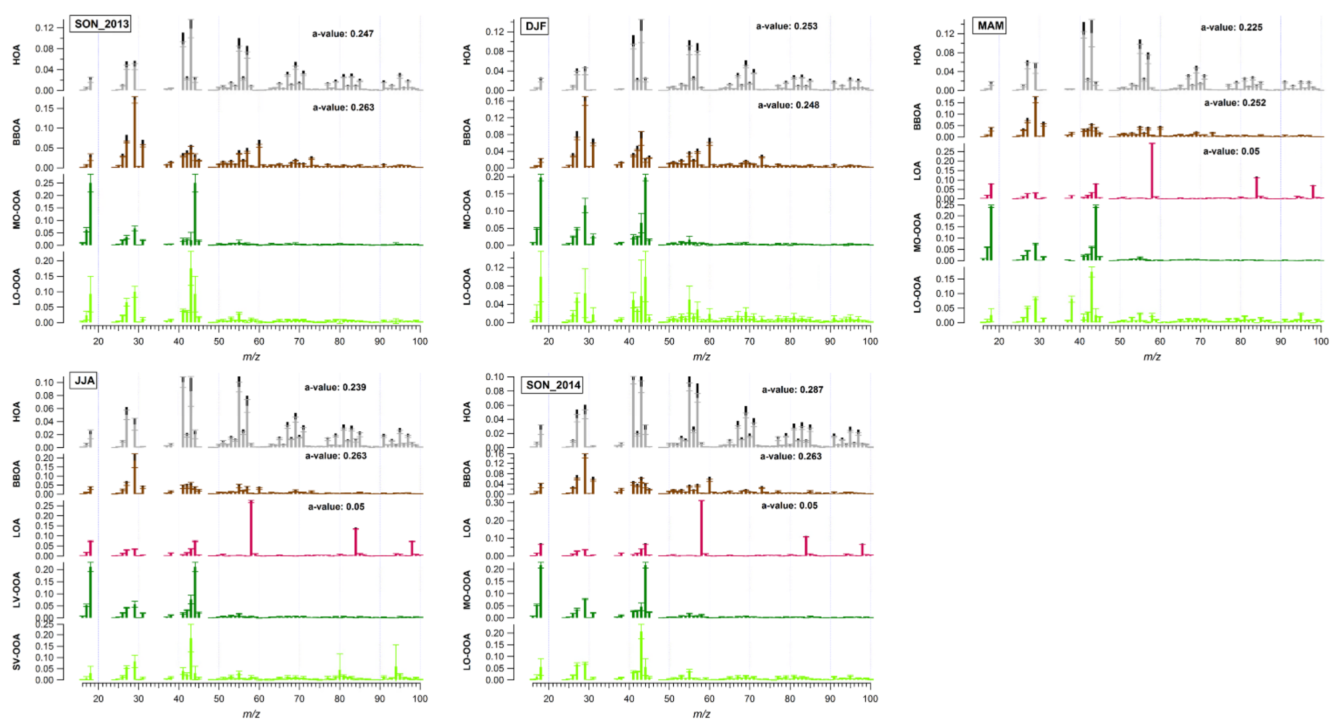

Fig. S6 Averaged factor profiles from bootstrap seasonal solutions for five different periods

Table S1 Criterion List for both seasonal and rolling PMF.

	Criterion	Type	Threshold
1	**HOA vs NO_x**	$R^2_{pearson}$, normal time series	p-value<0.05
2	**HOA vs eBC_{tr}**	$R^2_{pearson}$, normal time series	p-value<0.05
3	$\boldsymbol{EV_{60,BBOA}}$	Average, normal time series	p-value<0.05
4	**factor_4[44]**	Profiles, fraction, **sorting criterion**	>0
5	**factor_5[43]**	Profiles, fraction	>0

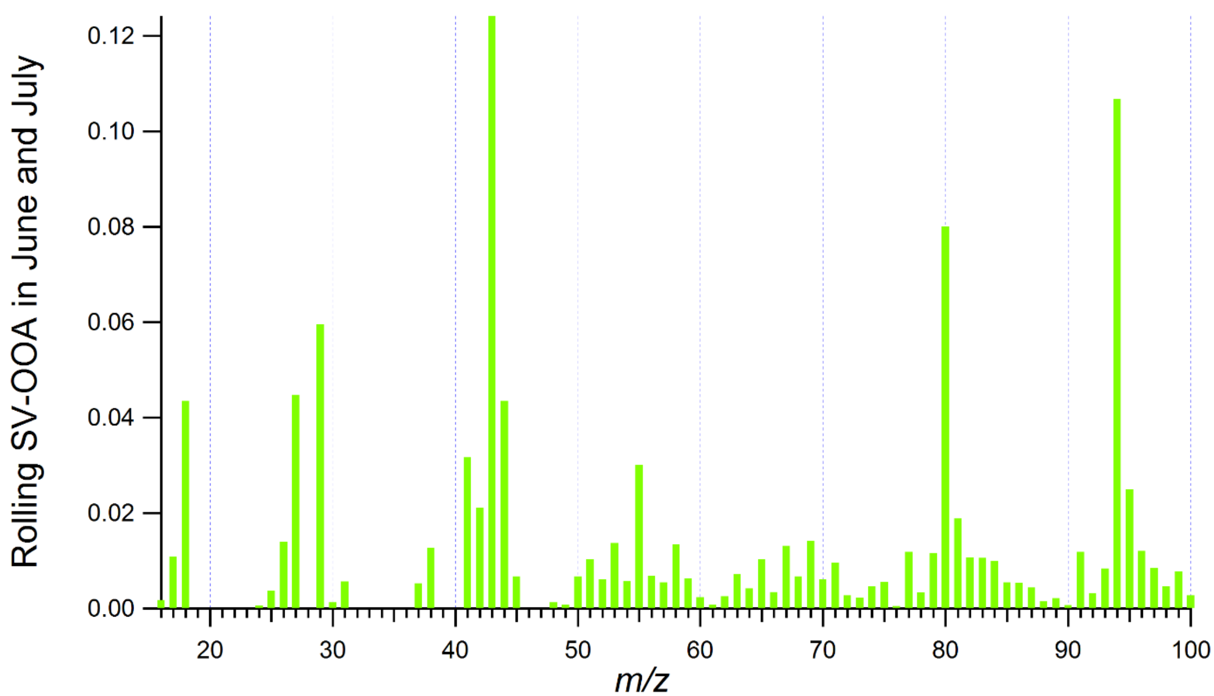

Fig. S7 Mass spectra for LO-OOA in June and July from rolling results

3 Employed *a*-values

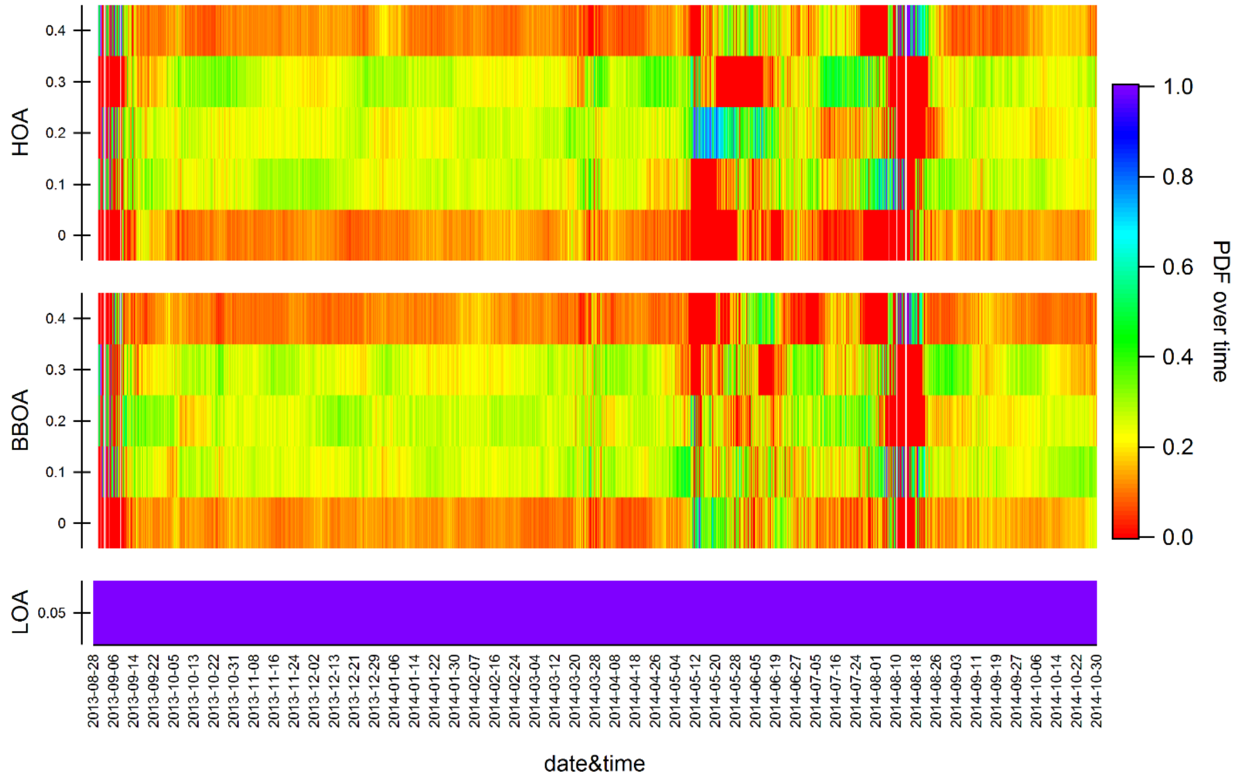

Fig. S8 The probability distribution of employed *a*-values for constrained factors as a function of time.

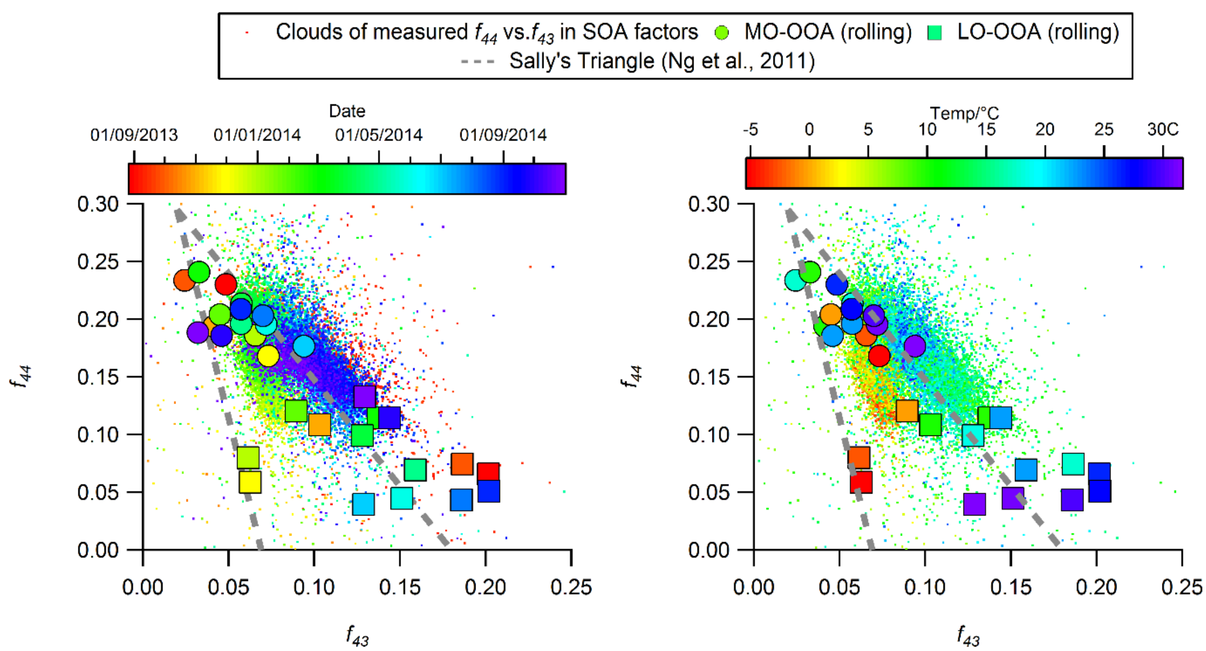

Fig. S9 OOA f_{44} vs. f_{43} for OOA factors in monthly resolution with colour coded by month and temperature.

4 Optimized time window size

We tested different time window size (1, 7, 14, and 28 days) and compared the solutions by applying same thresholds for the same criteria. We found optimum window sizes for this dataset is 14 days, with only 29 (0.15%) non-modelled points as shown in Fig. S10. The averaged Q/Q_{exp} for different time window sizes are similar, but the 14-day window solution still has the smallest Q/Q_{exp} (0.448). However, the Q/Q_{exp} for all window sizes are smaller than one, it is likely due to the high uncertainty from the measurement of ACSM (27/67 variables have S/N<2) and SoFi simplifies the equation of Q_{exp} to $n \times m$ because $n \times m >> p \times (n+m)$ when measured points are sufficiently large. Nevertheless, we selected and presented the 14-day window solution in this manuscript with its significant smaller missing points in the model.

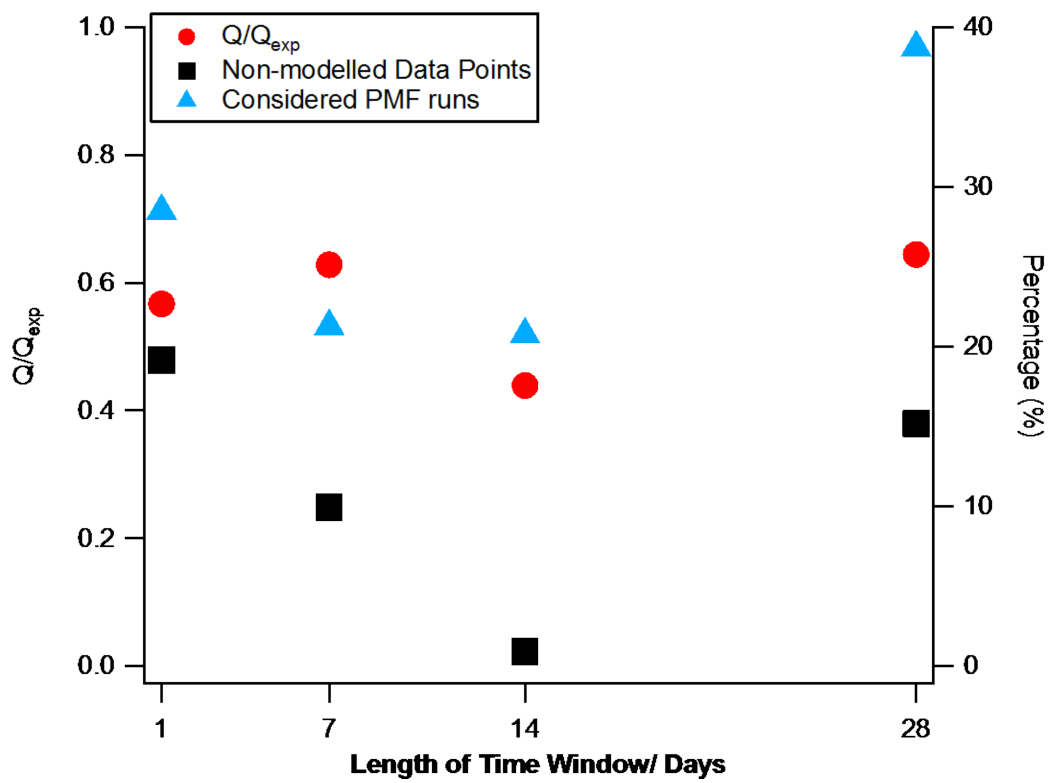

Fig. S10 Missing time points and Q/Qexp vs rolling window size (numbers still need to be updated)

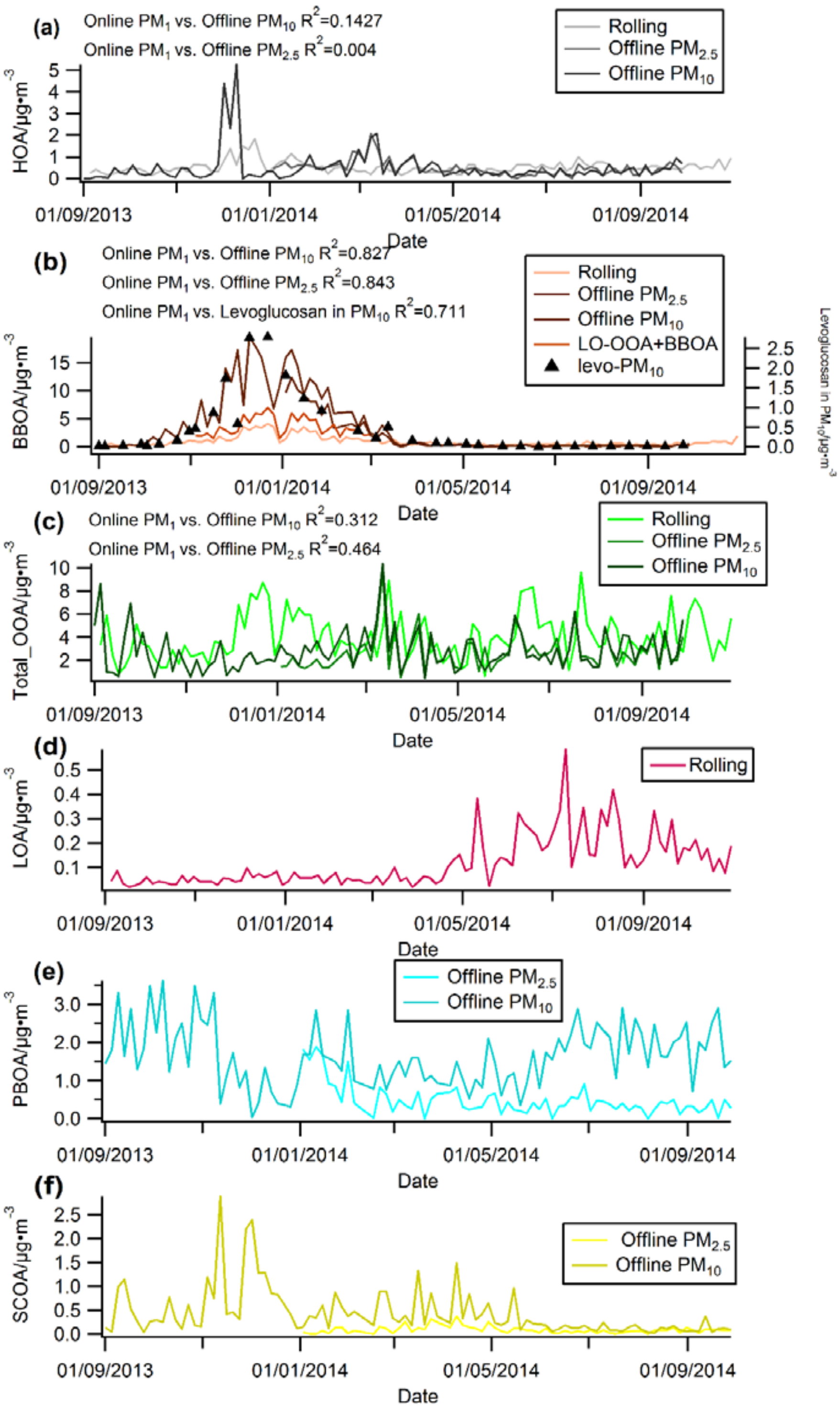

Fig. S11 The comparison between source apportionment results from offline AMS PM_{10}/$PM_{2.5}$ samples and online ACSM

References

Canonaco, F., Tobler, A., Chen, G., Sosedova, Y., Slowik, J. G., Bozzetti, C., Daellenbach, Kaspar Rudolf Haddad, I. El, Crippa, M., Huang, R.-J., Furger, M., Baltensperger, U. and Prevot, A. S. H.: A new method for long-term source apportionment with time-dependent factor profiles and uncertainty assessment using SoFi Pro: application to one year of organic aerosol data, Atmos. Meas. Tech. Discuss., doi:10.5194/amt-2020-204, 2020.

Crippa, M., Canonaco, F., Lanz, V. A., Äijälä, M., Allan, J. D., Carbone, S., Capes, G., Ceburnis, D., Dall'Osto, M., Day, D. A., DeCarlo, P. F., Ehn, M., Eriksson, A., Freney, E., Hildebrandt Ruiz, L., Hillamo, R., Jimenez, J. L., Junninen, H., Kiendler-Scharr, A., Kortelainen, A.-M., Kulmala, M., Laaksonen, A., Mensah, A. A., Mohr, C., Nemitz, E., O'Dowd, C., Ovadnevaite, J., Pandis, S. N., Petäjä, T., Poulain, L., Saarikoski, S., Sellegri, K., Swietlicki, E., Tiitta, P., Worsnop, D. R., Baltensperger, U. and Prévôt, A. S. H. H.: Organic aerosol components derived from 25 AMS data sets across Europe using a consistent ME-2 based source apportionment approach, Atmos. Chem. Phys., 14(12), 6159–6176, doi:10.5194/acp-14-6159-2014, 2014.

Drinovec, L., Močnik, G., Zotter, P., Prévôt, A. S. H., Ruckstuhl, C., Coz, E., Rupakheti, M., Sciare, J., Müller, T., Wiedensohler, A. and Hansen, A. D. A.: The “dual-spot” Aethalometer: An improved measurement of aerosol black carbon with real-time loading compensation, Atmos. Meas. Tech., 8(5), 1965–1979, doi:10.5194/amt-8-1965-2015, 2015.

Efron, B.: Bootstrap Methods: Another Look at the Jackknife, Ann. Stat., 7(1), 1–26 [online] Available from: https://www.jstor.org/stable/2958830, 1979.

Harrison, R. M., Beddows, D. C. S., Jones, A. M., Calvo, A., Alves, C. and Pio, C.: An evaluation of some issues regarding the use of aethalometers to measure woodsmoke concentrations, Atmos. Environ., 80, 540–548, doi:10.1016/j.atmosenv.2013.08.026, 2013.

Herich, H., Hueglin, C. and Buchmann, B.: A 2.5 year's source apportionment study of black carbon from wood burning and fossil fuel combustion at urban and rural sites in Switzerland, Atmos. Meas. Tech., 4(7), 1409–1420, doi:10.5194/amt-4-1409-2011, 2011.

Paatero, P.: User's guide for positive matrix factorization programs PMF2 and PMF3, Helsinki, Finland., 2010.

Petzold, A., Ogren, J. A., Fiebig, M., Laj, P., Li, S.-M., Baltensperger, U., Holzer-Popp, T., Kinne, S., Pappalardo, G., Sugimoto, N., Wehrli, C., Wiedensohler, A. and Zhang, X.-Y.: Recommendations for reporting "black carbon" measurements, Atmos. Chem. Phys., 13(16), 8365–8379, doi:10.5194/acp-13-8365-2013, 2013.

Sandradewi, J., Prévôt, A. S. H., Szidat, S., Perron, N., Alfarra, M. R., Lanz, V. A., Weingartner, E. and Baltensperger, U.: Using Aerosol Light Absorption Measurements for the Quantitative Determination of Wood Burning and Traffic Emission Contributions to Particulate Matter, Environ. Sci. Technol., 42(9), 3316–3323, doi:10.1021/es702253m, 2008.

Weingartner, E., Saathoff, H., Schnaiter, M., Streit, N., Bitnar, B. and Baltensperger, U.: Absorption of light by soot particles: determination of the absorption coefficient by means of aethalometers, J. Aerosol Sci., 34(10), 1445–1463, doi:10.1016/S0021-8502(03)00359-8, 2003.

Zotter, P., Herich, H., Gysel, M., El-Haddad, I., Zhang, Y., Močnik, G., Hüglin, C., Baltensperger, U., Szidat, S. and Prévôt, A. S. H.: Evaluation of the absorption Ångström exponents for traffic and wood burning in the Aethalometer-based source apportionment using radiocarbon measurements of ambient aerosol, Atmos. Chem. Phys., 17(6), 4229–4249, doi:10.5194/acp-17-4229-2017, 2017.